A Tyrosine Substitution in the Cavity Wall of a K Channel Induces an Inverted Inactivation

Göran Klement,* Johanna Nilsson,* Peter Århem,* and Fredrik Elinder†
*The Nobel Institute for Neurophysiology, Department of Neuroscience, Karolinska Institutet, SE-171 77 Stockholm, Sweden; and
†Department of Clinical and Experimental Medicine, Division of Cell Biology, Linköping University, SE-581 85 Linköping, Sweden

ABSTRACT Ion permeation and gating kinetics of voltage-gated K channels critically depend on the amino-acid composition of the cavity wall. Residue 470 in the *Shaker* K channel is an isoleucine, making the cavity volume in a closed channel insufficiently large for a hydrated K^+ ion. In the cardiac human ether-a-go-go-related gene channel, which exhibits slow activation and fast inactivation, the corresponding residue is tyrosine. To explore the role of a tyrosine at this position in the *Shaker* channel, we studied I470Y. The activation became slower, and the inactivation faster and more complex. At +60 mV the channel inactivated with two distinct rates ($\tau_1 = 20$ ms, $\tau_2 = 400$ ms). Experiments with tetraethylammonium and high K^+ concentrations suggest that the slower component was of the P/C-type. In addition, an inactivation component with inverted voltage dependence was introduced. A step to −40 mV inactivates the channel with a time constant of 500 ms. Negative voltage steps do not cause the channel to recover from this inactivated state ($\tau \gg 10$ min), whereas positive voltage steps quickly do ($\tau = 2$ ms at +60 mV). The experimental findings can be explained by a simple branched kinetic model with two inactivation pathways from the open state.

INTRODUCTION

An early inferred structural characteristic of voltage-gated K channels is a wide internal vestibule or cavity (1), later confirmed in crystallization studies (2). The volume, and consequently the amino-acid composition, of the wall of this cavity critically shapes the ion permeation and gating kinetics. Mutating residues pointing into the vestibule alter activation and inactivation kinetics. Because of its topological localization, the residue at the position corresponding to position 470 in the *Shaker* K channel plays an important role. In *Shaker* and most other voltage-gated K channels, this position is occupied by isoleucine, making the cavity volume in a closed channel insufficiently large for a hydrated K^+ ion or organic blockers (3,4). Replacing the isoleucine with the smaller alanine or cysteine shifts the conductance-versus-voltage ($G(V)$) curve in the positive direction along the voltage axis and (in combination with the T449V mutation) eliminates the C-type inactivation (4,5). In a few other K channels among vertebrate channels, notably human ether-a-go-go-related gene (hERG) and BK, the corresponding residues are aromatic. This fact is especially noteworthy for the hERG channel because this channel, important for repolarization of the heart action potential, exhibits strongly deviating activation and inactivation patterns compared with those of other Kv channels. The inactivation rate as well as recovery from the inactivated state are relatively fast, whereas the activation and deactivation rates are relatively slow, giving the channel inward-rectifying properties (6–10). Nevertheless, the inactivation has been suggested to be of C-type (8). The aromatic residue in hERG is tyrosine (Y652). The role of this residue for producing the specific features of hERG is only understood fragmentarily. Substituting Y652 and F656 leads to alterations in the C-type inactivation (11). Neither is the kinetic effect of substituting I470 in *Shaker* with tyrosine known; corresponding substitution with the aromatic tryptophan has been shown, however, to cause a negative shift of the $G(V)$ curve (5). Aromatic residues are also found in the corresponding position in the bacterial, voltage-independent channels KcsA and MthK (F103 and F87, respectively), which have been crystallized and structurally determined (2,12) and thus have made it possible to detail the location and position of the discussed residues in the vestibular wall (see Fig. 1).

To obtain information about the role of the tyrosine residue in the internal vestibule of hERG, and on the effect of aromatic residues in the vestibule of Kv channels in general, we replaced the isoleucine at position 470, corresponding to position 652 in hERG, with a tyrosine in a *Shaker* mutant lacking N-type inactivation (*Shaker* H4Δ6–46 (14,15) hereafter called ShIR). Our investigation showed that tyrosine in position 470 modifies both activation and inactivation kinetics, the rate of activation being decreased and the rate of the slow inactivation increased compared with that of *Shaker*. In addition, the substitution induces an inactivation component with an inverted voltage dependence; the mutant channel in the inverted inactivated state does not recover at voltages more negative than −40 mV, whereas it recovers rapidly at positive voltages. This type of inactivation seems unique, although at first sight it has features of a U-type inactivation.

Submitted August 15, 2007, and accepted for publication December 7, 2007.

Address reprint requests to Peter Århem, The Nobel Institute for Neurophysiology, Dept. of Neuroscience, Karolinska Institutet, SE-171 77 Stockholm, Sweden. Tel.: 46-8-524-869-03; E-mail: peter.arhem@ki.se.

Editor: Richard W Aldrich.

0006-3495/08/04/3014/09 $2.00

doi: 10.1529/biophysj.107.119842

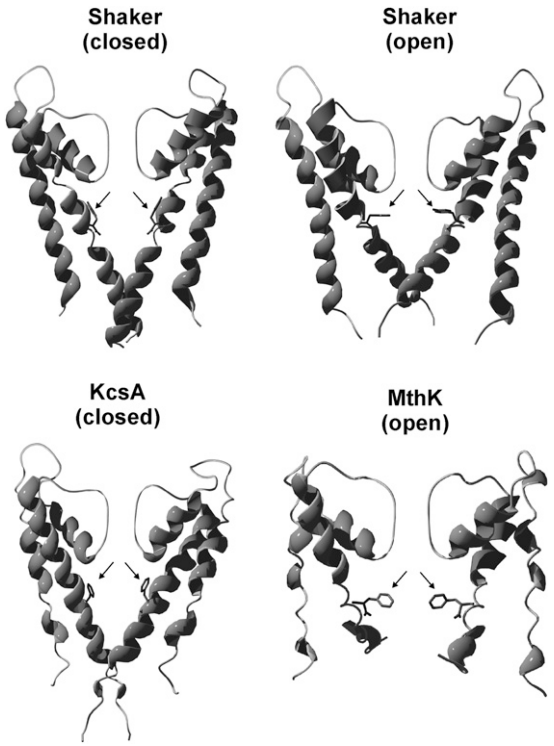

FIGURE 1 Hypothetical side-chain position of the tyrosine residue at position 470 in a three-dimensional model of *Shaker* in a closed and open state as envisioned by homology modeling (13). Corresponding aromatic residues in three-dimensional structures of the K channels KcsA (F103; accession No. 1BL8) and MthK (F87; accession No. 1LNQ) are shown in the lower panel.

METHODS

Molecular biology and channel expression

We used the ShIR channel (14) lacking the fast N-type inactivation (15). The mutations were made using a QuickChange site-directed mutagenesis kit (Stratagene, La Jolla, CA). cRNA was synthesized with a T7 mMessage mMachine kit (Ambion, Austin, TX) and injected into *Xenopus laevis* oocytes (20–5000 pg/cell). The oocytes were maintained at 12°C in a modified Barth's solution (MBS, in mM: 88 NaCl, 1 KCl, 2.4 $NaHCO_3$, 15 HEPES, 0.33 $Ca(NO_3)_2$, 0.41 $CaCl_2$, and 0.82 $MgSO_4$) adjusted to pH 7.6 by NaOH, and supplemented with penicillin (10 μg/ml) and streptomycin (10 μg/ml).

Electrophysiology

The electrophysiological experiments were carried out 2–4 days after injection of mRNA with a two-electrode voltage-clamp technique, using a CA-1 amplifier (Dagan, Minneapolis, MN). Microelectrodes were made from borosilicate glass and filled with a 3 M KCl solution. The resulting resistance varied between 0.5 and 2.0 MΩ. The currents were low-pass filtered at 1 kHz. All experiments were carried out at room temperature (20–22°C). For the electrophysiological experiments, Ringer's solution of the following composition was used (in mM): 88 NaCl, 1 KCl, 0.8 $MgCl_2$, 0.4 $CaCl_2$, and 15 HEPES adjusted by NaOH to reach pH 7.4. The final concentration of Na^+ is ~100 mM. The chemical substances were obtained from Sigma-Aldrich (Stockholm, Sweden, and Schnelldorf, Germany).

Kinetic modeling

Computer simulations of kinetic models were performed with in-house software. Table 1 shows equations and parameter values.

RESULTS

The I470Y substitution slows activation and speeds inactivation

Fig. 2 demonstrates the effect of the I470Y substitution on currents associated with rectangular voltage steps in 10-mV increments. At positive voltages, the monoexponential voltage-independent slow inactivation in ShIR ($\tau = 3.1 \pm 0.2$ s; $n = 3$) is replaced by two more rapidly inactivating components following a biexponential time course: 1), a voltage-independent component, speeded up >100-fold compared with the inactivation of ShIR ($\tau = 18 \pm 3$ ms; $n = 10$; Fig. 2, *B* and *C*); and 2), a somewhat slower voltage-dependent component ($\tau = 430 \pm 54$ ms at +60 mV; $n = 10$; Fig. 2, *B* and *C*). The recovery from the inactivation was about the same as that of ShIR (16,17). Fig. 2 *D* shows the time course of the recovery at −80 mV, yielding a time constant of ~1.0 s.

A further inactivation component became visible when a second pulse step to +40 mV was applied (Fig. 3 *A*). This inactivation component is most pronounced around −40 mV and disappears at higher voltages. It is also seen as a depression around −40 mV in the standard ''steady-state'' inactivation curve (Fig. 3 *B*) derived from the measurements in Fig. 3 *A*. The fact that this inactivation component is difficult to see in the one-pulse experiments in Fig. 2 *A* suggests that channels are trapped in the inactivated state at negative voltages and that the second (positive) pulse step in the two-pulse experiments in Fig. 3 *A* releases the channel from the inactivated state, making the time course of the inactivation visible. This explains the differential peak $G(V)$ curves obtained when one-pulse or two-pulse protocols were used (data not shown). Fig. 3 *C* shows the peak $G(V)$ curve, constructed from the measurements in Fig. 3 *A* (using a two-pulse protocol) in comparison with a standard $G(V)$ curve for ShIR. The main effect of the I470Y substitution on the curve is a shift of ~−10 mV.

The time course of the I470Y-induced inactivation at −40 mV is monoexponential, having a time constant of 483 ± 124 ms ($n = 3$) and reaching a steady-state level of 23 ± 7% ($n = 3$)

TABLE 1 Rate constants and parameters used in the model calculations

k_f, k_b	α, β	γ, δ	κ, λ	μ, ν	ε, φ	σ, τ
k_f, k_b (ms^{-1})	—	—	0.1, 1.0	—	—	0.003, 0.0002
k_{eq} (ms^{-1})	0.5	0.005	—	0.01	0.05	—
z_f	0.5	1.5	—	1.5	0.25	—
z_b	1.0	1.5	—	1.5	0.25	—
V_{eq}	−55	−80	—	−10	60	—

Forward rate constant k_f is calculated as $k_{eq} \exp((V - V_{eq}) \times z_f \times F \times R^{-1} \times T^{-1})$ and backward rate constant k_b as $k_{eq} \exp(-(V - V_{eq}) \times z_b \times F \times R^{-1} \times T^{-1})$. R, T, and F have their normal thermodynamic meanings.

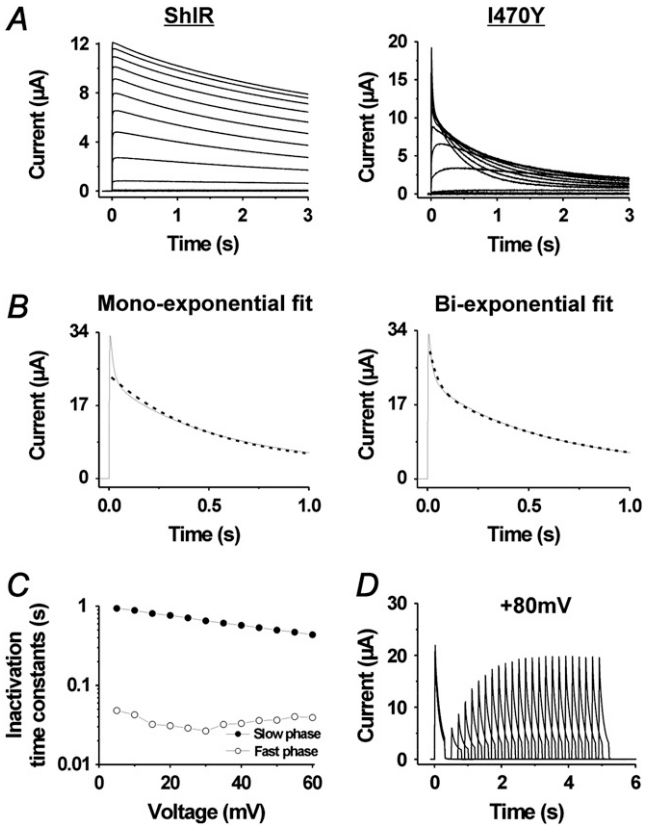

FIGURE 2 Effects of the I470Y substitution on ion currents. (*A*) Currents associated with depolarizations from −80 to +60 mV in increments of 10 mV for control ShIR and I470Y. (*B*) Test of exponential fits to the current associated with a voltage step to +60 mV. (*Left panel*) A monoexponential function fitted to the data. (*Right panel*) The sum of two exponentials fitted to the data. (*C*) Time constants of the two inactivation components induced at positive voltages, calculated from the recordings in *A*. (*D*) Time course of the recovery at −80 mV from the inactivation induced at +80 mV. $\tau = 1.0$ s.

of peak current (Fig. 4 *A*). The rate of activation at −40 mV in the I470Y channel is considerably slower than that of ShIR at corresponding open probability levels (−30 mV; see Fig. 3 *C*). Thus, whereas the activation $t_{½}$ for I470Y at −40 mV is 20 ± 7 ms ($n = 4$), the activation $t_{½}$ for ShIR at −30 mV is only 3.6 ± 0.7 ms ($n = 5$) (Fig. 4, *A* and *B*), thus sixfold faster. To highlight the voltage dependence of the I470Y-induced inactivation component just discussed, we plotted the quotient between steady-state current and peak current (I_{ss}/I_{peak}) against voltage (Fig. 4 *C*). The curve is clearly U-shaped around −40 mV, with the minimum at −43 mV, showing that this inactivation component in this respect resembles the U-type inactivation described previously for the *Shaker* channel (18). However, as already discussed, in contrast to the U-type inactivation of *Shaker*, the I470Y-induced inactivation does not disappear at negative voltages but does rapidly disappear at positive voltages, suggesting different mechanisms. We therefore refrained from using the term U-type for the I470Y-induced inactivation component at −40 mV.

In conclusion, introducing a tyrosine in the vestibule portion of the ShIR S6 at the same position as the tyrosine in the vestibule portion of S6 of hERG leads to a slowed channel opening at voltages around −40 mV and a faster inactivation, both at positive voltages (two components) and around −40 mV. Below, the characteristics of the inactivation components (of I470Y), especially the latter component, and their relations to the parent inactivation (in ShIR) are analyzed in more detail.

The inactivation component induced by a −40 mV pulse has a recovery pattern of reversed voltage dependence

Fig. 5 *A* shows the currents through I470Y channels associated by several consecutive steps to −40 mV from a holding voltage of −80 mV and applied with intervals of 3 s. Only the first pulse elicits a current that shows inactivation. An interpulse interval of 3 s is not sufficient to release the channel from the inactivated state, although this interval duration is clearly sufficient to release ShIR from a C-type inactivated state. Increasing the interval between the pulses up to 10 min did not change the situation; the I470Y channel did not recover from inactivation. We also tested pulses (of 1 s) down to −170 mV with no sign of recovery (Fig. 5 *B*).

However, Fig. 3 *A* clearly shows that the I470Y channel is not permanently trapped in the inactivated state. There are evidently pathways to escape from the inactivated state. At voltages more positive than −40 mV, the channel quickly recovers from the inactivated state. Fig. 5 *C* shows the recovery after a voltage step of varying amplitude, based on measurements using the protocol shown. The recovery curve obtained is reversed in comparison to the recovery curves for other inactivating channels (19,20). The peak current has fully recovered after a step to −10 mV or more positive.

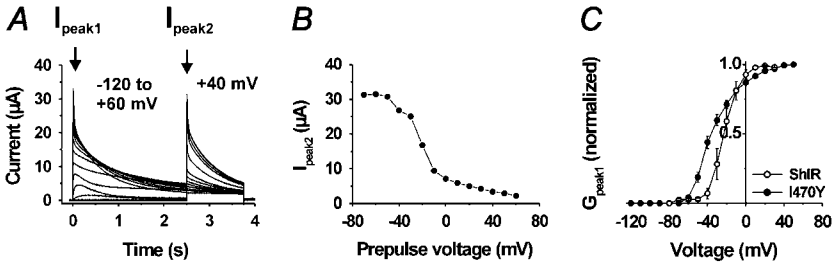

FIGURE 3 Activation and inactivation of the I470Y channel. (*A*) Currents associated with voltage steps from −120 to +60 mV in 10-mV increments, followed by a step to +40 mV. (*B*) Steady-state inactivation curve based on the recordings in *A*. (*C*) Peak-conductance curves for I470Y and ShIR, measured as $G_{peak1} = I_{peak1}/(V - E_K)$. Each point is the mean value from six or seven experiments.

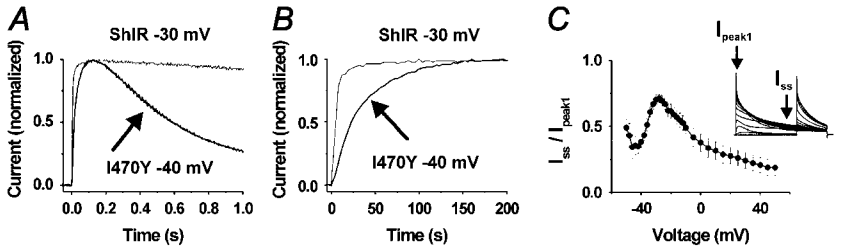

FIGURE 4 Characterization of currents in I470Y. (*A*) Comparison between the activation rates of I470Y and ShIR at approximately equal open probabilities (0.5). (*B*) Same as in *A* but at a faster time scale. (*C*) The quotient between current at 2.5 s and peak current-versus-voltage curve, showing the U-type resembling voltage dependence of the inverted inactivation component. Each point is the mean value from six or seven experiments.

Furthermore, the recovery at positive voltages is very fast, comparable to the activation of the channel. At +40 mV, 76 ± 9% ($n = 3$) of the channels had recovered within 2.5 ms (Fig. 5, *D* and *E*) corresponding to a time constant of 1.8 ms. A positive step forces the channel from the inactivated state occupied at −40 mV to an open state before it inactivates again. This is seen in Fig. 5 *D* as well as in Fig. 3 *B*. Thus, the channel does not go directly from the inactivated state with reversed voltage dependence to the more conventional inactivated state but passes an open state.

In conclusion, the I470Y substitution induces, at voltages around −40 mV, an inactivation with a voltage dependence of the recovery pattern that is reversed (or inverted) in comparison with previously described inactivation processes; the channel is trapped in the inactivated state when below −40 mV and rapidly recovers when above −40 mV. In the following, we refer to this inactivation component as the inverted inactivation component.

The different inactivation processes in I470Y are caused by different mechanisms

How are the inactivation components of I470Y related to previously described inactivation types? The most commonly studied slow inactivation mechanisms are the C-type and P-type inactivation. These inactivation types are assumed to

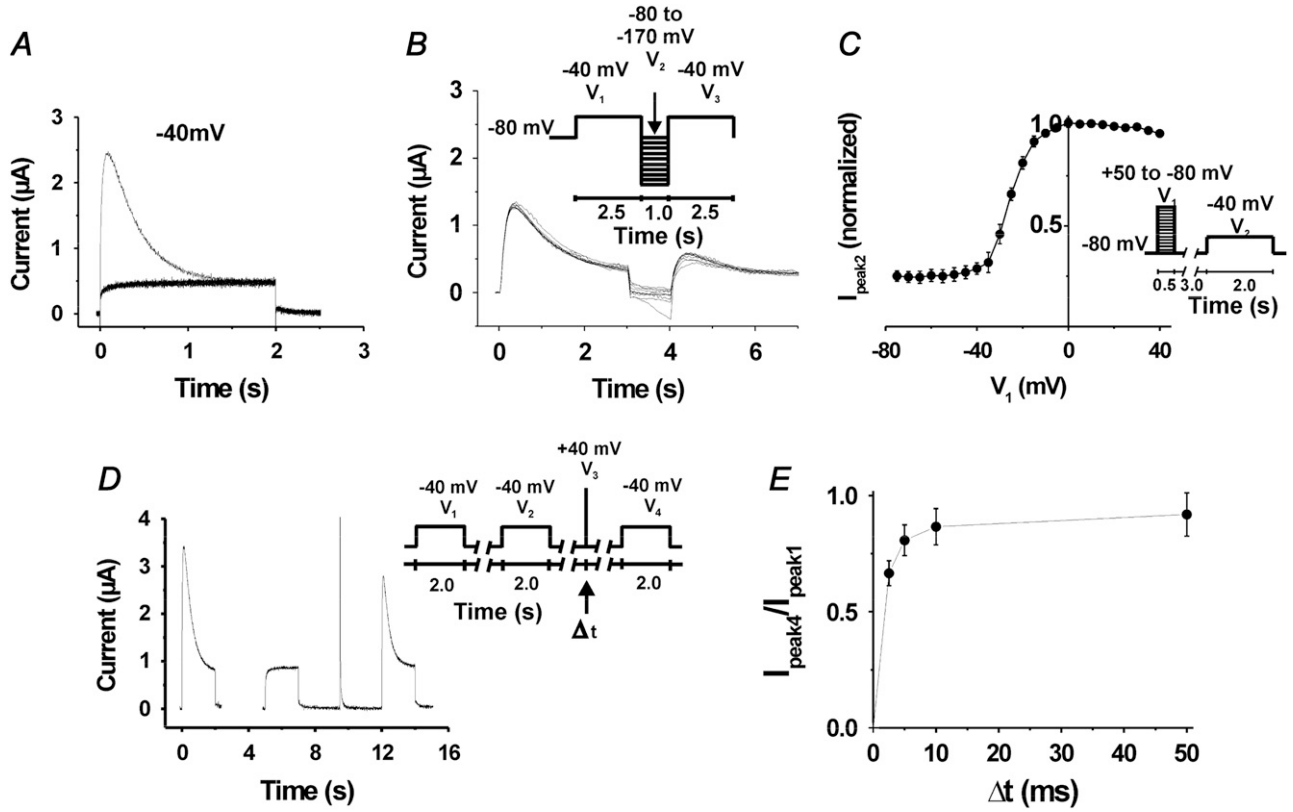

FIGURE 5 Voltage and time dependence of recovery from inverted inactivation in I470Y. (*A*) Lack of recovery in currents associated with voltage steps from −80 mV to −40 mV, repeated at a frequency of 0.2 Hz. (*B*) Lack of recovery from inactivation induced at −40 mV after pulse steps down to −170 mV. Superimposed currents. (*C*) Voltage dependence of recovery from the inactivation induced at −40 mV, measured as I_{peak2}/max I_{peak2}. (*D*) Recovery from the inactivation induced at −40 mV after a 2.5-ms duration pulse step to +40 mV ($\Delta t = 2.5$ ms). (*E*) The dependence of the recovery from inactivation on the duration ($\Delta t = 2.5$–50 ms) of a pulse step to +40 mV, measured as I_{peak4}/I_{peak1} (see *D*). Half-time value is 1.9 ms.

involve a conformational alteration or collapse of the ion-conducting pore, leading to a channel obstruction (21). The pore collapse has sometimes been referred to as P-type, and the later conformational change, stabilizing the inactivated state, has been referred to as C-type (16). The relation between the two forms is not fully understood. A prerequisite for the collapse is that K^+ ions escape from the selectivity filter. Prevention of this K^+ escape by increasing extracellular K^+ or by adding the K-channel blocker tetraethylammonium (TEA) slows down the pore constriction and the pore/collapse (P/C)-type inactivation (22–24). To investigate the I470Y inactivation components, we therefore added TEA or K^+ to the extracellular solution and measured the resulting currents.

Fig. 6, *A* and *B*, shows current families in control and 30 mM TEA solutions for the I470Y mutant with a two-pulse protocol used to release the channel from the inverted inactivated state. TEA has a very clear effect on the inactivation rate at positive voltages but hardly any effects on the inverted inactivation. Fig. 6 *C* shows a step to +60 mV for control, 10 mM TEA, and 30 mM TEA. TEA clearly retards (almost 10-fold) the slow phase of inactivation but has a much smaller (and opposite) effect on the fast phase (Fig. 6 *D*), suggesting that at least the I470Y slow component of the positive-voltage-induced inactivation is of the P/C type. In contrast, TEA has no effect on the inverted inactivation (Fig. 6, *E* and *F*). There is, however, a small effect on the activation that is connected with a modest TEA-induced shift of the $G(V)$ curve (data not shown).

Fig. 7 shows experiments with 100 mM K^+ solution, corresponding to the TEA experiments in Fig. 6, *A* and *B*. The figure demonstrates that the high K^+ concentration inhibits the slow, but not the fast, phase of the inactivation at positive voltages, as most clearly seen in Fig. 7 *C*. To detect a possible action on the inverted inactivation, we calculated $G(t)$ curves for the voltages around −40 mV (not shown). No systematic effect was found.

Altogether, these experiments suggest that the slow phase of the positive-voltage-induced inactivation is of P/C type,

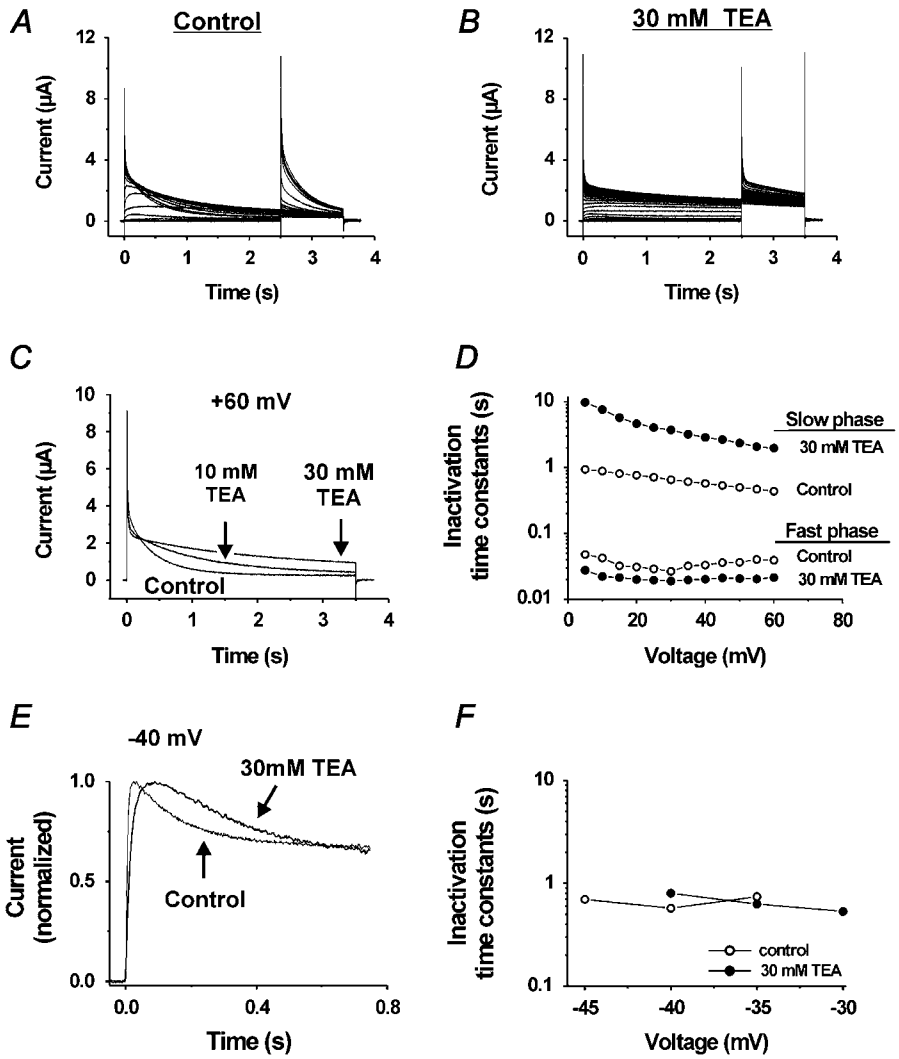

FIGURE 6 Effects of TEA on the inactivation components induced at high voltages. (*A* and *B*) Currents at steps between −80 and +60 mV from a holding voltage of −80 mV and a subsequent step to +40 mV in control (*A*) and 30 mM TEA (*B*). (*C*) Superimposed currents at +60 mV in varying concentrations of TEA, highlighting the decreased inactivation in high TEA concentration. (*D*) Effect of 30 mM TEA on time constants of the fast and slow inactivation components plotted versus voltage in the range from +5 to +60 mV, showing the difference in TEA effect on the two components. (*E*) Effect of 30 mM TEA on the current associated with a step to −40 mV. (*F*) Effect of 30 mM TEA on the inactivation time constant versus voltage curve.

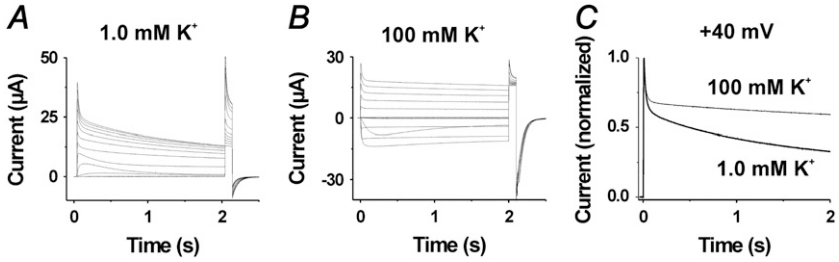

FIGURE 7 Effects of 100 mM K^+ solution on the inactivation components induced at high voltages. (*A* and *B*) Currents at steps between −80 and +40 mV from a holding voltage of −80 mV and a subsequent step to +40 mV in control (*A*) and in 100 mM K^+ solution (*B*). (*C*) Superimposed currents at +40 mV in control and 100 mM K^+ solution, highlighting the decreased inactivation in 100 mM K^+ solution.

whereas the inverted inactivation (and the fast phase of the positive-voltage-induced inactivation) is of another origin.

Kinetic modeling of the I470Y mutant

The basic features of these findings can be modeled by a relatively simple branched scheme with two separate inactivation pathways from the open state: one two-step forward pathway, explaining the biphasic inactivation time course at high potentials, and one two-step backward pathway, explaining the inactivation-trapped behavior at low threshold potentials (~−40 mV). Fig. 8 *A* shows the model, and Table 1 lists the rate constants and associated parameter values. C denotes closed states, O the open state, and I inactivated states. The horizontal transitions are voltage dependent whereas the vertical are not. The model assumes four independent voltage sensors responsible for the transitions from C_1 to C_5. The opening step ($C_5 \rightarrow O_6$) is slower and more voltage dependent than the previous steps in the activation pathway. In total, nine elementary charges are moved to open this model channel, in relative agreement with the number estimated for *Shaker* WT 12 charges (25). The open channel is assumed to equilibrate quickly with the I_6 state. This transition is voltage independent and biased toward the open state with a factor of 10. (I_6 could also be assumed to be a conducting state with only minor differences in currents.) The $I_5 \rightarrow I_6$ transition has the same voltage dependence as $C_5 \rightarrow O_6$ and is almost equally fast. However, although $C_5 \rightarrow O_6$ is biased toward O_6 at −40 mV, $I_5 \rightarrow I_6$ is biased toward I_5. The two transitions are shifted 70 mV in relation to each other (see Table 1), causing the channel to enter I_5 with a high degree of probability at −40 mV. From O_6, the channel quickly and voltage-dependently inactivates to I_{7P} at positive voltages. From I_{7P}, there is a further slow and voltage-independent inactivation step to I_{7C}. Thus, a channel in I_5 will stay trapped in this state at negative voltages but will rapidly reenter O_6 at positive voltages, from where it moves to I_{7C} and I_{7P}.

Compared with a corresponding model of *Shaker* WT, the I470Y model differs in three respects: it assumes two extra states of inactivation (I_5 and I_6), other values for the inactivation transitions $O_6 \rightarrow I_{7P}$ and $I_{7P} \rightarrow I_{7C}$, and for the last activation step $C_5 \rightarrow O_6$. The I470Y model was constructed to reproduce the features presently studied and does not claim to be complete; e.g., it does not explain the fast recovery from inactivation associated with positive potentials. Thus, there must be a pathway from I_{7C} to C_1 without passing O_6. Probably there is also a pathway from O_6 to C_1 without passing C_5 on deactivation. Fig. 8 *B* shows a highly schematic view of

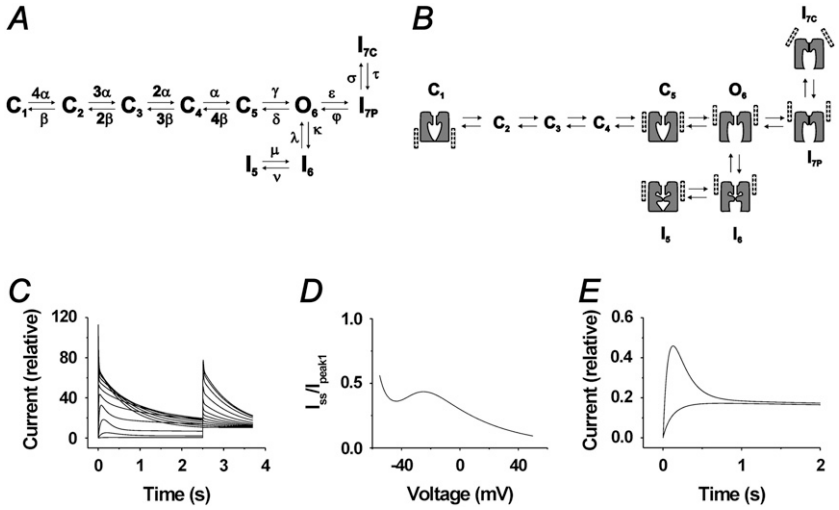

FIGURE 8 Kinetic modeling of the I470Y mutant. (*A*) The kinetic scheme used for the calculations. C denotes closed states, O an open state, and I inactivated states. Rate constant symbols indicated. See Table 1 for parameter values. (*B*) Schematic structural model of the kinetic model, showing hypothetical movements of voltage sensors, selectivity filter, and internal gate. The different positions of the voltage sensors in I_{C7} and I_{P7} are based on a scenario suggested by Loots and Isacoff (16). (*C*) Calculated time evolution of the model current at voltage steps in increments of 10 mV followed by a step to +40 mV (cf. Fig. 3 *A*). (*D*) Calculation of I_{ss}/I_{peak1} from *C* (cf. Fig. 4 *C*). (*E*) Calculation of currents associated with two consecutive steps to −40 mV from a holding potential of −80 mV. The traces are superimposed to illustrate that the channel model is trapped in an inactivated state (cf. Fig. 5 *A*).

tentative molecular correlates. Fig. 8 *C* shows the currents corresponding to the experimental measurements in Fig. 3 *A*, calculated from the model. Fig. 8 *D* shows the quotient between steady-state current and peak current (I_{ss}/I_{peak}) against voltage, corresponding to the curve in Fig. 4 *C*. Fig. 8 *E* shows currents corresponding to the experimental measurements in Fig. 5 *A*.

DISCUSSION

Kv channels exhibit a broad spectrum of inactivation phenotypes with varying kinetics, ranging from very fast (N-type) to slow (P/C- and U-type), and with different underlying mechanisms. The N-type inactivation is caused by an intracellular pore-plugging mechanism (15,26) and the P/C type by a selectivity filter collapse (23,27,28). The mechanism of the U-type inactivation (18,29) remains unclear, although a role for the T1 domain has been implicated (30).

Our investigation shows that a tyrosine substitution in the S6 segment at position 470 of the ShIR channel induces a faster and more complex inactivation pattern compared with that of ShIR, which is mainly of the P/C type. The I470Y-induced inactivation comprises 1), a fast voltage-independent and 2), a slower but still relatively fast voltage-dependent component at positive voltages, and 3), a component at voltages around −40 mV that shows no recovery at voltages more negative than −40 mV but a very fast recovery at positive voltages. The latter component thus shows a reversed voltage dependence of the recovery pattern compared with that of ShIR. Experiments with TEA and high K^+ concentrations suggest that the different inactivation components in this mutant depend on different underlying mechanisms; the voltage-dependent component at positive voltages are possibly of P/C type. No other substitution at position 470 has been reported to cause similar effects (3–5). The substitution I470Y also induces a slower activation around −40 mV. In conclusion, the I470Y substitution thus induces both a slower activation and a faster inactivation within a certain voltage range. At first sight this suggests induction of hERG-like features. However, quantitatively these induced features clearly deviate from those characterizing hERG; the induced slowing of activation is not comparable to the slow activation seen in hERG, and the rate of inactivation of the fast component is still much slower than that of hERG. Furthermore, replacing the tyrosine in the 652 position in hERG with alanine has no marked effects on the gating kinetics of the hERG channel (11).

The mechanisms of the I470Y inactivation components

The size and chemical character of the residue in position 470 are crucial for a number of functional features of *Shaker*. They determine the functional size of the internal vestibule (3), they influence C-type inactivation (4,31), and they regulate the tendency of the channel to become defunct at removal of K^+ ions on both sides of the membrane (3). The ShIR isoleucine (as is similar-sized leucine) is large enough to prevent the closure of the channel if a hydrated K^+ ion is located in the cavity, causing a gating current tail with a slowly rising phase (3). ShIR also C-type inactivates and becomes defunct at K^+ removal (32). The smaller residues, alanine and cysteine, enlarge the cavity, allowing a hydrated K^+ ion, or even a TEA molecule, to reside in the cavity when the channel is closed (3,4). They also shift the $G(V)$ curve in a positive direction (4,5). Alanine and cysteine mutant channels do not C-type inactivate (in combination with T449V) and cannot become defunct (32). The bulkier tyrosine or tryptophan delimit the cavity size further, compared with ShIR isoleucine, and shift the $G(V)$ curve in negative direction (5) (present investigation). Tyrosine and tryptophan mutant channels C-type inactivate, but their tendency to become defunct is still unexplored.

We find intriguing similarities between the defunct state and the inverted inactivation state of the I470Y channel. The sequence of events leading to a defunct channel includes 1), a depolarization step that allows the K^+ ions to escape from the selectivity filter, 2), a step to −40 mV that leads to accumulation of channels in alternative closed states, inaccessible in the presence of K^+, and 3), a subsequent step to −80 mV, which moves back the S4 to a resting state. In the defunct channel, the S4 can still move to some extent, but the channel cannot open because of a conformational change in the selectivity filter, which affects the last step of the S4 movement. Recovery from the defunct state is possible after long depolarizations in the presence of K^+ (33). The similarities between the defunct and inverted inactivation states are evident: the importance of an opening step (O_6 in the model) and of intermediate, alternative, closed states (at −40 mV) (I_6) for entering the state and for the impossibility to escape from it (I_5) at hyperpolarization.

How does the introduced tyrosine induce the novel inactivation components in the mutant channel? We find it intriguing that the aromatic residues corresponding to hERG Y652 in the closed KcsA and the open MthK point in different directions and therefore shape the internal vestibule wall differently (see Fig. 1). One is pointing upward toward the selectivity filter (KcsA), and the other is pointing toward the center of the cavity (MthK). One possible scenario is that the different tyrosine configurations in I470Y are state dependent, the upward position being associated with the closed state and the cavity-pointing position with the open state (see the *Shaker* homology models in open and closed state; Fig. 1), and that the induced inverted inactivation process depends on the configuration alterations. As seen in the schematic diagram in Fig. 8 *B*, this would mean that the cavity-pointing tyrosine position is found in the inactivated state I_6. At intermediate potentials (~−40 mV), the channel will move into the I_5 state, from which it can escape only when the channel is sufficiently depolarized to push Y470 into the upright position

(in state O_6). We suggest that state I_5 bears some resemblance to the alternative closed state, leading to the defunct state (32); but for escape from the defunct state, reintroduction of K^+ is also needed.

The I470Y substitution is also associated with a biphasic inactivation at positive voltages, the slow phase of which is most likely of C-type. A coupling between C-type inactivation and the tendency to become defunct has been suggested (34). How the different inactivation components in the I470Y mutant are related, and how the tyrosine residue affects the selectivity filter, remain to be explored.

What gating mechanisms are causing the different inactivation processes in the mutant channel? The P/C-type-like inactivation component is possibly caused by a tyrosine-induced destabilization of the selectivity filter in agreement with the conclusions from previous studies of P/C-type inactivation regarding the structural changes of the selectivity filter (16). Concerning the inverted inactivation component, we find three scenarios conceivable: tyrosine 1), interacts directly with the hydrated ion in the vestibule because of its cavity-pointing position in state I_5 (see Figs. 1 and 8 *B*), 2), interacts indirectly and allosterically destabilizes the selectivity filter, or 3), modifies the gating process at the bundle crossing or at the glycine hinge. All the alternatives are speculative, but the first alternative seems least likely, considering the small effect on the permeation path the aromatic residues at corresponding positions have in KcsA and MthK. In both cases, the aromatic residues do not appear to constitute steric, electrostatic, or reaction field barriers (35). If the inverted inactivation state has some resemblance to the defunct state, the most likely scenario seems to be the third alternative, that tyrosine causes this effect by allosterically modifying the gating process (3).

This work was supported by grants from the Swedish Research Council (Project 13043 and 15083), the Swedish Society of Medicine, the Swedish Society for Medical Research, the KI foundation, Åke Wibergs Stiftelse, Magn. Bergvalls Stiftelse, the Swedish Heart-Lung Foundation, and the County Council of Östergötland.

REFERENCES

1. Armstrong, C. M. 1971. Interaction of tetraethylammonium ion derivatives with the potassium channels of giant axons. *J. Gen. Physiol.* 58: 413–437.
2. Doyle, D. A., J. Morais Cabral, R. A. Pfuetzner, A. Kuo, J. M. Gulbis, S. L. Cohen, B. T. Chait, and R. MacKinnon. 1998. The structure of the potassium channel: molecular basis of K^+ conduction and selectivity. *Science.* 280:69–77.
3. Melishchuk, A., and C. M. Armstrong. 2001. Mechanism underlying slow kinetics of the OFF gating current in *Shaker* potassium channel. *Biophys. J.* 80:2167–2175.
4. Holmgren, M., P. L. Smith, and G. Yellen. 1997. Trapping of organic blockers by closing of voltage-dependent K^+ channels: evidence for a trap door mechanism of activation gating. *J. Gen. Physiol.* 109:527–535.
5. Hackos, D. H., T. H. Chang, and K. J. Swartz. 2002. Scanning the intracellular S6 activation gate in the *Shaker* K^+ channel. *J. Gen. Physiol.* 119:521–532.
6. Yellen, G. 1999. The bacterial K^+ channel structure and its implications for neuronal channels. *Curr. Opin. Neurobiol.* 9:267–273.
7. Sanguinetti, M. C., C. Jiang, M. E. Curran, and M. T. Keating. 1995. A mechanistic link between an inherited and an acquired cardiac arrhythmia: HERG encodes the IKr potassium channel. *Cell.* 81: 299–307.
8. Smith, P. L., T. Baukrowitz, and G. Yellen. 1996. The inward rectification mechanism of the HERG cardiac potassium channel. *Nature.* 379:833–836.
9. Spector, P. S., M. E. Curran, A. Zou, M. T. Keating, and M. C. Sanguinetti. 1996. Fast inactivation causes rectification of the IKr channel. *J. Gen. Physiol.* 107:611–619.
10. Schonherr, R., and S. H. Heinemann. 1996. Molecular determinants for activation and inactivation of HERG, a human inward rectifier potassium channel. *J. Physiol.* 493:635–642.
11. Chen, J., G. Seebohm, and M. C. Sanguinetti. 2002. Position of aromatic residues in the S6 domain, not inactivation, dictates cisapride sensitivity of HERG and eag potassium channels. *Proc. Natl. Acad. Sci. USA.* 99:12461–12466.
12. Jiang, Y., A. Lee, J. Chen, M. Cadene, B. T. Chait, and R. MacKinnon. 2002. Crystal structure and mechanism of a calcium-gated potassium channel. *Nature.* 417:515–522.
13. Chanda, B., O. K. Asamoah, R. Blunck, B. Roux, and F. Bezanilla. 2005. Gating charge displacement in voltage-gated ion channels involves limited transmembrane movement. *Nature.* 436:852–856.
14. Kamb, A., L. E. Iverson, and M. A. Tanouye. 1987. Molecular characterization of *Shaker*, a *Drosophila* gene that encodes a potassium channel. *Cell.* 50:405–413.
15. Hoshi, T., W. N. Zagotta, and R. W. Aldrich. 1990. Biophysical and molecular mechanisms of *Shaker* potassium channel inactivation. *Science.* 250:533–538.
16. Loots, E., and E. Y. Isacoff. 1998. Protein rearrangements underlying slow inactivation of the *Shaker* K^+ channel. *J. Gen. Physiol.* 112:377–389.
17. Elinder, F., R. Männikkö, and H. P. Larsson. 2001. S4 charges move close to residues in the pore domain during activation in a K channel. *J. Gen. Physiol.* 118:1–10.
18. Klemic, K. G., G. E. Kirsch, and S. W. Jones. 2001. U-type inactivation of Kv3.1 and *Shaker* potassium channels. *Biophys. J.* 81:814–826.
19. Timpe, L. C., T. L. Schwarz, B. L. Tempel, D. M. Papazian, Y. N. Jan, and L. Y. Jan. 1988. Expression of functional potassium channels from *Shaker* cDNA in *Xenopus* oocytes. *Nature.* 331:143–145.
20. Hodgkin, A. L., and A. F. Huxley. 1952. The dual effect of membrane potential on sodium conductance in the giant axon of *Loligo*. *J. Physiol.* 116:497–506.
21. Kurata, H. T., and D. Fedida. 2006. A structural interpretation of voltage-gated potassium channel inactivation. *Prog. Biophys. Mol. Biol.* 92:185–208.
22. Grissmer, S., and M. Cahalan. 1989. TEA prevents inactivation while blocking open K^+ channels in human T lymphocytes. *Biophys. J.* 55:203–206.
23. Lopez-Barneo, J., T. Hoshi, S. H. Heinemann, and R. W. Aldrich. 1993. Effects of external cations and mutations in the pore region on C-type inactivation of *Shaker* potassium channels. *Receptors Channels.* 1:61–71.
24. Choi, K. L., R. W. Aldrich, and G. Yellen. 1991. Tetraethylammonium blockade distinguishes two inactivation mechanisms in voltage-activated K^+ channels. *Proc. Natl. Acad. Sci. USA.* 88:5092–5095.
25. Schoppa, N. E., K. McCormack, M. A. Tanouye, and F. J. Sigworth. 1992. The size of gating charge in wild-type and mutant *Shaker* potassium channels. *Science.* 255:1712–1715.
26. Zhou, M., J. H. Morais-Cabral, S. Mann, and R. MacKinnon. 2001. Potassium channel receptor site for the inactivation gate and quaternary amine inhibitors. *Nature.* 411:657–661.
27. Hoshi, T., W. N. Zagotta, and R. W. Aldrich. 1991. Two types of inactivation in *Shaker* K^+ channels: effects of alterations in the carboxy-terminal region. *Neuron.* 7:547–556.

28. Cordero-Morales, J. F., L. G. Cuello, Y. Zhao, V. Jogini, D. M. Cortes, B. Roux, and E. Perozo. 2006. Molecular determinants of gating at the potassium-channel selectivity filter. *Nat. Struct. Mol. Biol.* 13:311–318.

29. Klemic, K. G., C. C. Shieh, G. E. Kirsch, and S. W. Jones. 1998. Inactivation of Kv2.1 potassium channels. *Biophys. J.* 74:1779–1789.

30. Kurata, H. T., G. S. Soon, J. R. Eldstrom, G. W. Lu, D. F. Steele, and D. Fedida. 2002. Amino-terminal determinants of U-type inactivation of voltage-gated K^+ channels. *J. Biol. Chem.* 277:29045–29053.

31. Olcese, R., D. Sigg, R. Latorre, F. Bezanilla, and E. Stefani. 2001. A conducting state with properties of a slow inactivated state in a *Shaker* K(+) channel mutant. *J. Gen. Physiol.* 117:149–163.

32. Melishchuk, A., A. Loboda, and C. M. Armstrong. 1998. Loss of *Shaker* K channel conductance in 0 K^+ solutions: role of the voltage sensor. *Biophys. J.* 75:1828–1835.

33. Gomez-Lagunas, F. 1997. *Shaker* B K^+ conductance in Na^+ solutions lacking K^+ ions: a remarkably stable non-conducting state produced by membrane depolarizations. *J. Physiol.* 499:3–15.

34. Loboda, A., A. Melishchuk, and C. Armstrong. 2001. Dilated and defunct K channels in the absence of K^+. *Biophys. J.* 80:2704–2714.

35. Jogini, V., and B. Roux. 2005. Electrostatics of the intracellular vestibule of K^+ channels. *J. Mol. Biol.* 354:272–288.